

Status of the Transverse Multibunch Modes in PEP-II *

J. Scott Berg

Abstract

In [Ber95b], I computed multibunch mode growth rates for the PEP-II *B* Factory. Since then, I have updated the broadband impedance model [BR95b, Ber96a], Robert Rimmer has measured the cavity modes in the high power test cavity, and Yunhai Cai has supplied updated lattice parameters. I am also using a slightly different model for the feedback [Ber96a], and I have included a way to estimate the effects of chromaticity. Finally, I have made more detailed computations regarding the expected effect of Landau damping. Putting all these together, the results from computing the growth rates of the multibunch modes in the PEP-II *B* Factory are given, and the conditions necessary to assure stability are discussed.

1 Introduction

The method described in [Ber96a] is used to compute the growth rates of multibunch modes in the PEP-II *B* Factory. I use the program described in [Ber96b]. This method differs from the usual methods for computing multibunch growth rates in that it takes into account coupling between the multibunch modes. A slightly simpler version of this method has been previously presented in other places [BR95a, BR95b].

2 Parameters

The parameters to be used here are given in table 1. Three values will be used for the number of buckets M : 873 (every fourth bucket), 1164 (every third bucket), and 1746 (every other bucket; the nominal value). The current will always be increased by the ratio of 1746/1658, since there are 1658 filled buckets in the nominal case (see [Ber96a] for the reason for this). Table 2 gives a list of the combinations of E , I , and N_{cav} which will be used.

Potential-well distortion will be taken into account. Table 3 gives the values of the bunch length, synchrotron tune, and tune-shift at the longitudinal emittance that will be used in these computations [Hei].

3 Impedance Model

The Impedance Model used here is essentially the same as that of [Ber95b]. There have been some changes in the model used, and many of the parameter values have changed. [Ber96a] uses a model very close to this one, but the parameters here are slightly different, and also include both rings and both planes of transverse motion.

3.1 Resistive Wall

The resistive wall impedance is given by the formula

$$Z_{\perp}^{\text{RW}}(\omega) = -i\sqrt{2} \frac{R_{\text{RW}}}{\sqrt{-i\omega/\omega_0}}, \quad (1)$$

*Work supported by Department of Energy contract DE-AC03-76SF00515.

description	symbol	LER		HER		units
		horizontal	vertical	horizontal	vertical	
betatron tune	ν_β	38.57	36.64	24.618	23.638	nm-rad s
emittance	ϵ	64.43	2.57	48.24	1.93	
damping time	τ	0.0583	0.0576	0.0370	0.0368	
nominal synchrotron tune	ν_s	0.03362246		0.05207387		MeV MeV GeV A MHz
momentum compaction	η_C	$1.23204608115 \times 10^{-3}$		2.41241×10^{-3}		
Energy loss per turn	ΔE	0.789988		3.588748		
Maximum rf voltage	\hat{V}	5.1		18.5		
energy	E	*		*		
total current	I	*		*		
number of cavities	N_{cav}	*		*		
rf frequency	f_{rf}	476				
rf harmonic number	h_{rf}	3492				
number of bunches	k_B	*				
buckets in symmetric fill	M	*				
nominal bunch length	σ_ℓ	1				cm
circumference	L	2199.318				m

Table 1: Parameters for the PEP-II rings [PEP93, Cai]. A * indicates that this parameter will be discussed in the text.

Ring	E (GeV)	I (A)	N_{cav}
LER	3.109	2.254	6
LER	3.109	2.254	8
LER	3.109	3.159	6
LER	3.109	3.159	8
LER	2.5	3.159	6
LER	2.5	3.159	8
HER	9	1.043	20
HER	9	1.043	24

Table 2: Parameter combinations that will be considered. The currents given here are increased by the ratio 1746/1658 from their real values (2.14 A, 3 A, and 0.99 A respectively).

where R_{RW} is given by

$$R_{\text{RW}} = F \frac{Z_0 L_p}{2\pi b_p^3} \sqrt{\frac{2c}{\omega_0 \sigma Z_0}} = F \frac{Z_0 L_p}{2\pi b_p^3} \sqrt{\frac{c^2}{2\pi \omega_0 \sigma}}. \quad (2)$$

Here b_p is the smallest half-dimension (vertical or horizontal) of the vacuum chamber, L_p is the length of the vacuum chamber, σ is the vacuum chamber wall conductivity, Z_0 is the impedance of free space ($\approx 377\Omega$), and F is a form factor which depends only on the shape of the vacuum chamber [GvZZ93].

The arc sections of the low-energy ring vacuum chamber are elliptical with a major axis of 3.740 inches and a minor axis of 2.170 inches [PEPa]. This geometry makes F 0.4219 in the horizontal direction, and 0.8263 in the vertical direction [GvZZ93]. The vacuum chamber is made of 6063 T5 aluminum alloy [PEPa], which has a resistivity of $1/\sigma = 32 \Omega\text{-nm}$ [ASM90]. The lengths of the low-energy ring arc sections can be estimated to be the same as those of the high energy ring arc sections (see below), giving 1490.482 m [Dal]. Thus, R_{RW} for the arc sections is 460 k Ω /m horizontally and 902 k Ω /m vertically.

The straight sections of the low-energy ring vacuum chamber are round with a diameter of 3.5 in. [PEPb]. F is 1 for this geometry [GvZZ93]. The vacuum chamber is made of 304 stainless steel [Hun], giving a resistivity of $1/\sigma = 720 \Omega\text{-nm}$ [ASM90]. The length of the straight sections is 708.836 m (see below). Thus, R_{RW} for the straight sections is 560 k Ω /m.

Ring	E (GeV)	I (A)	M	σ_ℓ (cm)	$\Delta\nu_s \times 10^4$	ν_s
HER	9	1.043	873	1.03	2.58	0.0484
HER	9	1.043	1164	1.02	1.99	0.0500
HER	9	1.043	1746	1.01	0.89	0.0505
LER	3.109	2.254	873	1.20	0.35	0.0252
LER	3.109	2.254	1164	1.15	7.43	0.0259
LER	3.109	2.254	1746	1.105	6.45	0.0276
LER	3.109	3.159	873	1.27	-12.10	0.0235
LER	3.109	3.159	1164	1.21	-0.64	0.0245
LER	3.109	3.159	1746	1.14	4.98	0.0262
LER	2.5	3.159	873	1.34	-23.13	0.0222
LER	2.5	3.159	1164	1.26	-8.70	0.0235
LER	2.5	3.159	1746	1.18	4.54	0.0252

Table 3: Bunch length, synchrotron tune, and tune shift due to potential-well distortion [Hei]. Tune shift is the synchrotron tune shift at the longitudinal emittance, and includes the tune shift due to the nonlinearity in the rf potential. The longitudinal emittance is the emittance with the bunch length shown in this table.

The arc sections of the high-energy ring vacuum chamber can be modelled as being rectangular with a height of 5 cm and a width of 9 cm [Ng]. Thus, F is 0.822101 vertically and 0.402180 horizontally [GvZZ93]. The vacuum chamber is made of copper, giving a resistivity of $1/\sigma = 17.1 \text{ } \Omega\text{-nm}$ [ASM90]. The length of the arc sections is 1490.482 m [Dal] (the arc sections are considered to extend to the VAT valves). Thus, R_{RW} for the arc sections is 410 k Ω /m horizontally and 838 k Ω /m vertically.

The straight sections of the high-energy ring vacuum chamber the same geometry and material as the low-energy ring vacuum chamber. The length of the straight sections is 708.836 m (this number includes the IR chamber length). Thus, R_{RW} for the straight sections is 560 k Ω /m.

3.2 Inductive

The inductive part of the transverse impedance in the low-energy ring is obtained by scaling the longitudinal inductive impedance of 83.3 nH [HKL⁺95] by $2c/\omega b_p^2$ [Cha93], where b_p is a characteristic dimension of the beam pipe. Worst-case values are obtained by performing this scaling with $b_p = 2.7559$ cm for the low energy ring and $b_p = 2.5$ cm for the high energy ring (the vertical size of the arc section chamber [PEPa, Ng]).

The impedance will not be constant for all frequencies; it is expected to begin to roll off at high frequencies. Since the average behavior at high frequencies is expected to be similar to that of a cavity, a high-frequency roll-off of $\omega^{-3/2}$ is assumed [Hei]. The form for the transverse impedance is thus

$$Z_{\perp}^{\text{Ind}}(\omega) = \frac{-iR_{\text{Ind}}}{(1 - i\omega/\omega_C)^{3/2}}, \quad (3)$$

where R_{Ind} is the transverse impedance associated with the inductance. To determine the cutoff frequency ω_C , the loss factor from Z_{\perp}^{Ind} is computed as a function of ω_C , and compared to the total loss factor from inductive components of 2.9 V/pC [Hei]. The total loss factor is

$$-i\frac{L}{2\pi} \int_{-\infty}^{\infty} e^{-\omega^2\sigma_\tau^2} \frac{\omega d\omega}{(1 - i\omega/\omega_C)^{-3/2}}, \quad (4)$$

where L is the inductance (a Gaussian bunch has been assumed). Using the bunch length of 1 cm, this formula gives the right loss factor when $\omega_C \approx 24.1$ GHz. Note that $R_{\text{Ind}} = 2cL/b_p^2$.

Plane	Frequency ω_R GHz	Q	R_{res} k Ω /m
horizontal	1.068	25	15.931
horizontal	1.120	31	0.092
horizontal	1.205	723	8.442
horizontal	1.346	323	31.199
horizontal	1.425	414	58.688
horizontal	1.540	73	1.987
horizontal	1.599	146	7.831
horizontal	1.670	377	75.775
horizontal	1.738	320	0.127
horizontal	1.766	2664	4.903
vertical	0.792	115	34.916
vertical	1.063	27	16.911
vertical	1.133	54	0.162
vertical	1.202	871	10.135
vertical	1.327	611	58.328
vertical	1.420	1138	160.689
vertical	1.542	92	2.508
vertical	1.595	145	7.777
vertical	1.676	783	153.796
vertical	1.723	446	0.177
vertical	1.749	1317	2.414

Table 4: Cavity higher order modes for PEP-II high power test cavity [Rim]. These are preliminary values.

3.3 Cavity Tails

It is well known that the longitudinal impedance of a single cavity rolls off at high frequency as $\omega^{-1/2}$ [HK89]. A simple model with the appropriate high-frequency roll-off is

$$Z_{\parallel}^{\text{Tail}}(\omega) = iR_{\text{Tail}} \left[\left(1 + \frac{\omega}{\omega_C + i\alpha} \right)^{-1/2} - \left(1 - \frac{\omega}{\omega_C - i\alpha} \right)^{-1/2} \right]. \quad (5)$$

This model is fit to a model of the cavity run through ABCI for $m = 1$ [Chi94, HKL+95] with the known higher order modes removed. The parameters are found to be $R_{\text{Tail}} = 45.1344$ k Ω /m², $\omega_C = 2.4$ GHz, and $\alpha = 1.34722$ GHz [Ber95a]. This impedance must of course be multiplied by the number of cavities.

The longitudinal impedance (5) is scaled by $\beta_0 c/\omega$ to obtain the transverse impedance [Cha93, Ber96a].

3.4 Cavity Higher Order Modes

A preliminary list of the cavity higher order modes is given in table 4. Each mode is considered to be a single resonator of the form [Cha93]

$$Z_{\perp}^{\text{res}}(x\omega_R) = \frac{R_{\text{res}}}{x + iQ(1 - x^2)}. \quad (6)$$

These impedances must of course be multiplied by the number of cavities.

3.5 BPM Resonance

The beam position monitors (BPM's) also have a resonance. Horizontally, the resonance is at 7.05 GHz with an R_{res} of 281 Ω /m per BPM and a Q of 60. Since there are 300 BPM's, the total R_{res} is 84 k Ω /m [Ng]. Vertically, it is at 6.2 GHz, with a Q of about 200, and a total R_{res} for all the BPM's of 120 k Ω /m [Ng].

Region	LER $\langle\beta_x\rangle$ (m)	LER $\langle\beta_y\rangle$ (m)	HER $\langle\beta_x\rangle$ (m)	HER $\langle\beta_y\rangle$ (m)
Entire ring	17.3810	18.3647	27.1485	24.7775
Arc sections	14.8544	16.3061	16.7016	21.5983
Straight sections	22.0700	22.1851	46.7627	30.7466
Cavities	*	*	*	*
BPM's	17.0329	16.6291	23.8357	23.8627

Table 5: Average β -functions for various impedance sources and regions. The arc sections are considered to extend from the end of the last element before the first arc bend in each arc section through the end of the last arc bend in each arc section. The straight sections are the remainder of the ring. Entries with a * are discussed in the text.

Ring	N_{cav}	$\langle\beta_x\rangle$ (m)	$\langle\beta_y\rangle$ (m)
LER	6	9.4443	20.0286
LER	8	9.6644	17.8720
HER	20	13.5111	14.8817
HER	24	13.5811	14.7845

Table 6: Average β -functions for the cavities.

3.6 Average β -functions

Each impedance must be multiplied by the β -function, averaged over the region where the impedance is [Ber96a]. If the impedance is from a discrete object, such as the cavities or the BPM's, then the average β -function is obtained by summing the β -functions at each occurrence of the object, and dividing by the number of objects. If the impedance is from an object which has a finite length which is not small compared to the betatron wavelength, such as for resistive-wall impedances or the summarized inductance, then one computes the integrals of the β -functions over that region. In practice, this integral is computed by using a lattice file (supplied in this case by Yunhai Cai), taking the β -functions at various points, and using trapezoid-rule integration to perform the integral. The results are summarized in table 5.

The average β -functions at the cavities are a special case. In the low-energy ring, if there are 6 cavities, they will be placed in the positions labeled CAV3, CAV4, and CAV5 in the lattice file [Sch]. If there are 8 cavities, the two extra will be placed in the positions labeled CAV2. In the high-energy ring, if there are 20 cavities instead of 24, the cavities will be removed from the positions labeled CAV5[A-D].08. Then table 6 gives the average β -functions for various relevant cases.

4 Landau Damping

Landau damping can be expected from tune shift with amplitude both in transverse and longitudinal dimensions. The transverse tune shifts that can be expected are shown in table 7. The longitudinal tune shifts that can be expected were shown in table 3. The transverse damping rates are mostly negligible when compared with the radiation damping rate. The largest source of Landau damping will be from the nonlinearity in the longitudinal potential, especially when potential-well distortion is included.

Using the formulas given in [ZCB86] (equations (IV.5.23-28), and the discussion in section IV.6), one can determine if the $m = 1$ modes of the beam are stable or not in the presence of tune shift with amplitude in the longitudinal direction. One first determines the real and imaginary parts of the coherent frequency using the method of [Ber96a, Ber96b]. One then uses the method described in [ZCB86] to find whether the $m = 1$ modes are stable with Landau damping, using the appropriate tune shift with amplitude given in table 3. This amounts to asking whether the modes are on the stable or unstable side of the diagram in figure 1.

As can be seen from figure 1, if the frequency shift of the coherent mode is large enough, and in particular if it is in the opposite direction of the tune shift with amplitude, then there is little or no Landau damping.

Tune	Amplitude	Tune shift
LER ν_x	$J_x = \epsilon_x$	-7.08×10^{-6}
LER ν_x	$J_y = \epsilon_y$	-1.77×10^{-7}
LER ν_y	$J_x = \epsilon_x$	-4.43×10^{-6}
LER ν_y	$J_y = \epsilon_y$	-1.37×10^{-6}
HER ν_x	$J_x = \epsilon_x$	-3.42×10^{-6}
HER ν_x	$J_y = \epsilon_y$	-1.68×10^{-6}
HER ν_y	$J_x = \epsilon_x$	-4.20×10^{-5}
HER ν_y	$J_y = \epsilon_y$	-5.89×10^{-7}

Table 7: Tune shifts at various amplitudes [Cai, Ber96a].

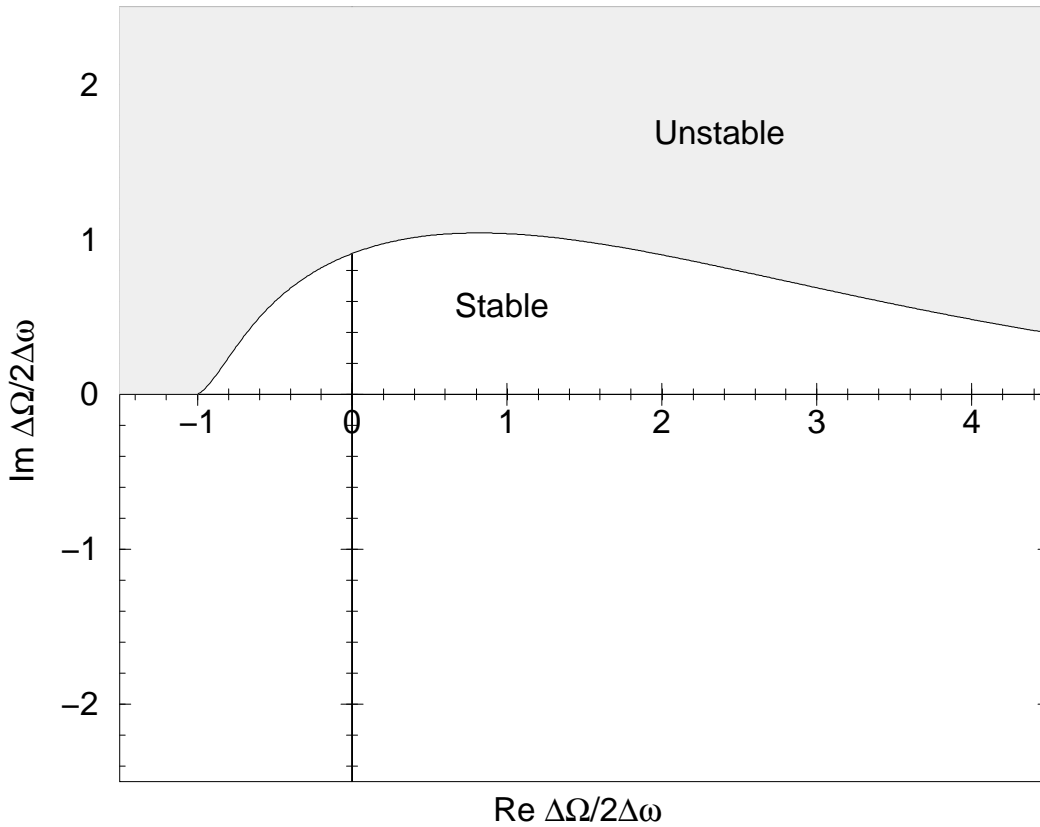


Figure 1: Stability diagram for Landau damping [ZCB86]. If the complex frequency shift for an $m = 1$ mode computed by the method of [Ber96a, Ber96b] is in the shaded region, the $m = 1$ mode is unstable.

5 Method for Analysis

I begin by computing the growth rates for the multibunch modes, up through the $m = 3$ modes. An example of this is shown in figure 2. Next, I add sufficient feedback to damp the $m = 0$ modes to radiation

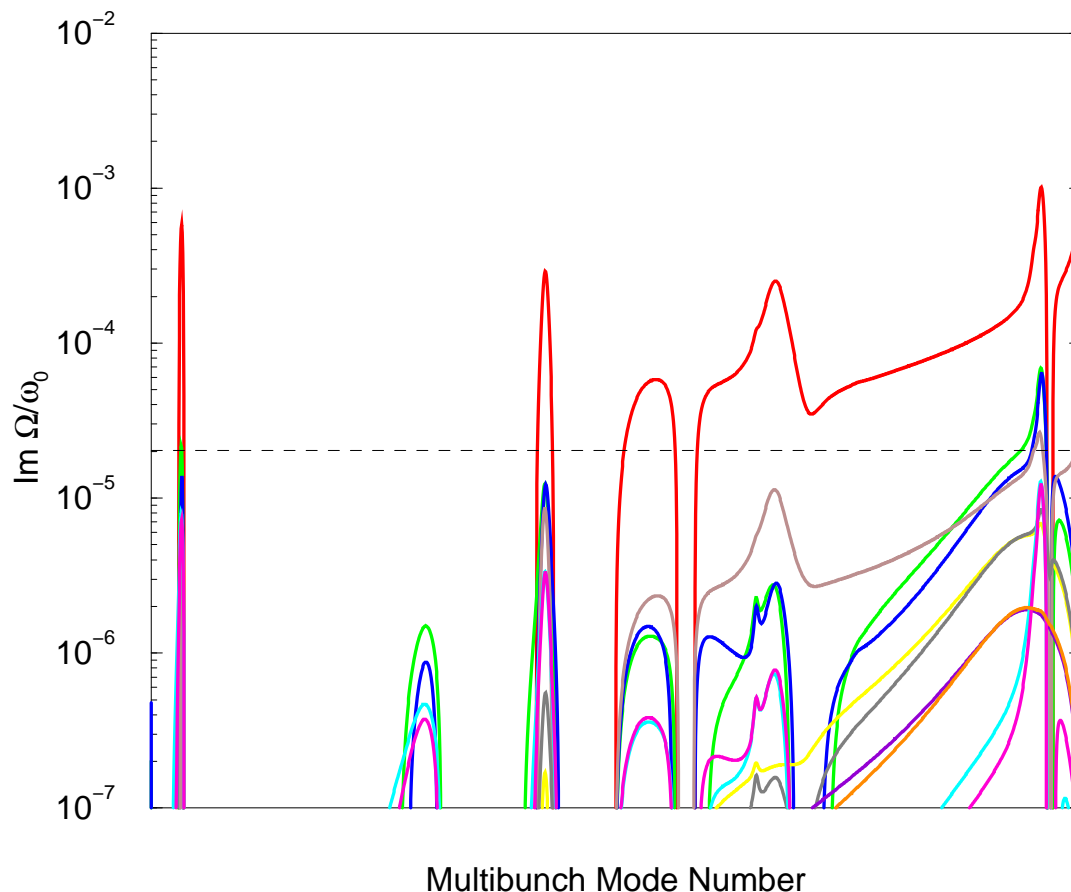


Figure 2: Multibunch modes without correction. Plotted are the growth rates versus mode number. The example shown is for the case of the vertical plane in the LER at 3.109 GeV, 2.254 A, and 6 cavities. The dashed line is the radiation damping rate.

damping. An example is shown in figure 3.

If there are $m = 1$ modes which are still not below the radiation and/or Landau damping levels, then the following procedure is used:

1. If necessary, the chromaticity of the ring is increased so as to reduce the growth rates from the BPM resonance. If growth rates due to the BPM resonance alone are above the damping rates, it will be impossible to get stability by simply de- Q -ing cavity modes. Even if the growth rates due to the BPM resonance are just below the damping rates, if the cavity modes overlap the modes driven by the BPM resonance, the cavity modes would need to be de- Q -ed drastically to get the combination below the damping rate.
2. If possible (usually only in the horizontal plane), the chromaticity is increased to so as to reduce all modes below the damping rate.
3. If necessary, the cavity modes are de- Q -ed by reducing the Q and the R_{res} by the same factors. They are de- Q -ed until they exactly equal the appropriate damping rate. This is done using a multidimensional

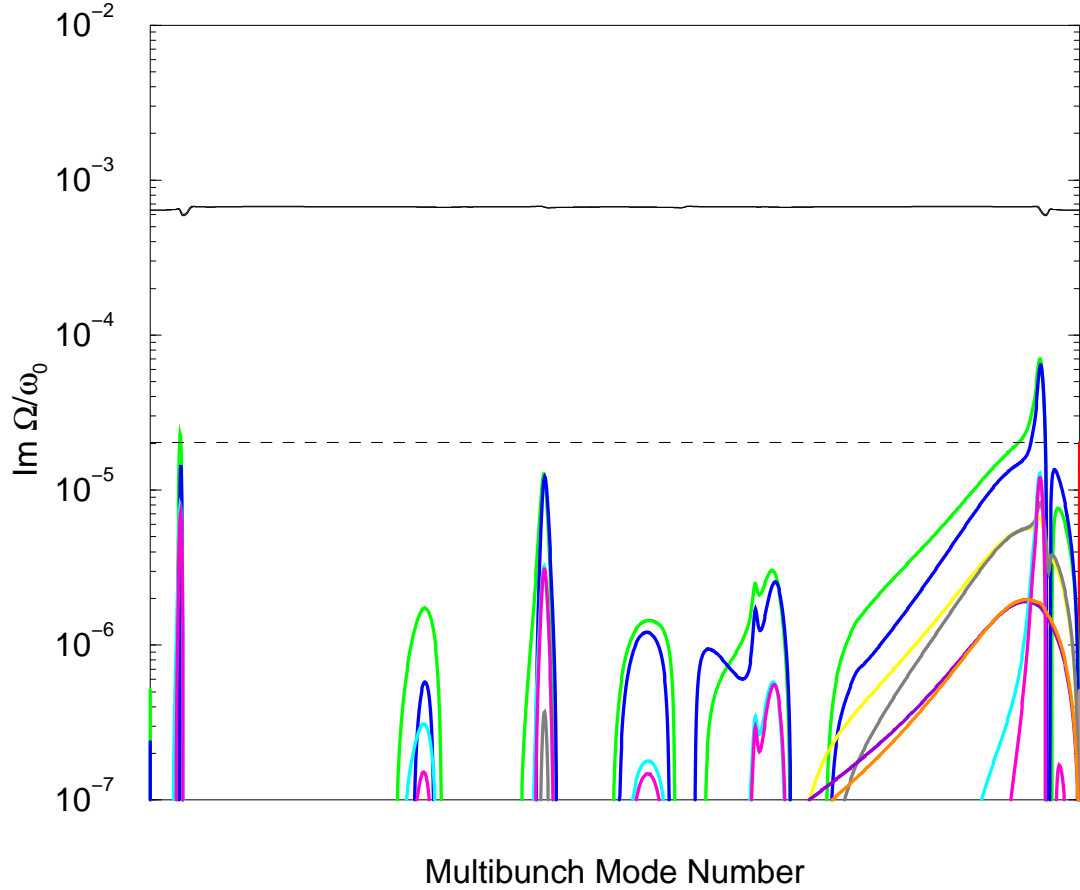


Figure 3: Multibunch modes with feedback. Compare figure 2. The thin solid line is the damping rate due to Landau damping for the $m = 1$ modes.

secant method where the cavity mode de- Q ing factor is being varied so as to make the peaks of the ratio of the growth rates to the damping rates in various regions equal to 1.

6 Results and Analysis

When Landau damping from the longitudinal tune shift with amplitude is considered, most of the cases are stable. For the cases which are unstable, the necessary de- Q ing is shown in table 8. It is preferred that the maximum chromaticity that we run at is 2 [Cai], but that puts unrealistically large requirements on the damping that is necessary. A chromaticity of 3 is the maximum realistic chromaticity [Cai]. It is clear that if the BPM resonance is as large as what is used in this computation, one should run at the largest realistic chromaticity, at least for the conditions shown in table 8.

Cho Ng is currently working on getting more accurate calculations of the BPM resonance impedance. If his improved results indicate that the resonance is not as strong, then the effects due to the BPM resonance may be negligible. Table 9 shows the results if the BPM resonance is removed. The best results are generally obtained when running at one of the extremes of chromaticity, taken to be -3 and 2 [Cai]. There is a tradeoff

Ring	Plane	N_{cav}	E (GeV)	I (A)	M	ξ	1327	1420	1676
LER	vertical	6	3.109	2.254	873	2	1.73	1.64	5.17
LER	vertical	8	3.109	2.254	873	2	2.41	2.11	6.97
LER	vertical	6	3.109	2.254	873	3	1.14	1.51	3.34
LER	vertical	8	3.109	2.254	873	3	1.56	1.94	4.59
LER	horizontal	8	3.109	3.159	1164	1.09	–	–	–
LER	vertical	6	3.109	3.159	1164	2	1.10	2.29	4.52
LER	vertical	8	3.109	3.159	1164	2	1.32	2.82	6.17
LER	vertical	6	3.109	3.159	1164	3	–	2.10	3.74
LER	vertical	8	3.109	3.159	1164	3	1.17	2.59	4.66
LER	vertical	6	3.109	3.159	1746	2	–	1.80	14.69
LER	vertical	8	3.109	3.159	1746	2	1.13	2.20	18.49
LER	vertical	6	3.109	3.159	1746	3	–	1.63	7.57
LER	vertical	8	3.109	3.159	1746	3	1.04	2.01	9.65
LER	horizontal	8	2.5	3.159	1746	2.13	–	–	–
LER	vertical	6	2.5	3.159	1746	2	1.20	2.27	26.75
LER	vertical	8	2.5	3.159	1746	2	1.47	2.74	37.06
LER	vertical	6	2.5	3.159	1746	3	1.05	1.99	9.96
LER	vertical	8	2.5	3.159	1746	3	1.27	2.46	12.67

Table 8: De-Qing necessary to fix instability due to cavity higher-order modes. The numbers in the last 3 columns indicate the factor by which the Q and R_{res} of the corresponding cavity mode must be reduced to achieve stability. Cavity modes are labeled by the frequency in megahertz of the vertical cavity mode.

involved in changing the chromaticity. Since the real part of the impedance doesn't fall off until extremely high frequencies, increasing the chromaticity gives a damping effect from the real part of the broadband impedance. However, the cavity higher-order modes have frequencies below the peak of the $m = 1$ form factor, and thus as chromaticity is increased, their growth rates increase as well. Thus, it is not always clear whether one wants to run at negative or positive chromaticity, although one probably wants to run at one extreme or the other. Since the 1676 MHz mode seems to be the worst, and it seems generally better off with positive chromaticity, then one should probably try to run with the maximum positive chromaticity, at least for the unstable cases listed in tables 8 and 9.

Assuming that we get the tune shift with amplitude given in table 3 has one problem. Consider the plot shown in figure 4. If the tune shift with amplitude is negative, then there is a large current at which it goes through zero. At this point, there will be no Landau damping. Thus, if current is slowly increased in the ring, one may not be able to rely on any Landau damping, at least from the longitudinal tune shift with amplitude.

7 Conclusions and Commentary

We have demonstrated that with Landau damping due to potential-well distortion, the high-energy ring is stable for all operating conditions, as is the horizontal plane of the low-energy ring with suitable adjustments of chromaticity in a couple of cases. In the vertical plane, 2.14 A and 3.109 GeV appear to be stable operating conditions as well, at least if the bunches are in every other bucket or every third bucket. A significant amount of cavity mode de-Qing is necessary to achieve for the operating conditions listed in table 8. There are several operating conditions which are stabilized by Landau damping from a negative tune shift with amplitude, but one must question whether one those conditions will be stable at intermediate currents.

A more thorough analysis could answer this last point by actually computing the modes for several values of the current as one increases to the operating current. One should make the synchrotron tune and bunch length change appropriately as the current increases.

One should attempt to quantify if there is any Landau damping from bunch-to-bunch tune spread, and how that interacts with other sources of Landau damping.

Ring	Plane	N_{cav}	E (GeV)	I (A)	M	ξ	1327	1420	1676
LER	vertical	6	3.109	2.254	873	-3	1.06	1.06	3.10
LER	vertical	8	3.109	2.254	873	-3	1.31	1.16	3.66
LER	vertical	6	3.109	2.254	873	0	1.07	1.66	3.04
LER	vertical	8	3.109	2.254	873	0	1.41	2.01	3.84
LER	vertical	6	3.109	2.254	873	2	-	1.88	2.48
LER	vertical	8	3.109	2.254	873	2	1.05	2.30	2.97
LER	vertical	6	3.109	3.159	1164	-3	-	2.28	5.43
LER	vertical	8	3.109	3.159	1164	-3	-	2.57	6.36
LER	vertical	6	3.109	3.159	1164	0	1.17	4.64	6.37
LER	vertical	8	3.109	3.159	1164	0	1.33	5.61	8.40
LER	vertical	6	3.109	3.159	1164	2	1.07	3.81	4.57
LER	vertical	8	3.109	3.159	1164	2	1.29	4.78	6.33
LER	vertical	6	3.109	3.159	1746	-3	-	1.09	3.60
LER	vertical	8	3.109	3.159	1746	-3	-	1.24	4.44
LER	vertical	6	3.109	3.159	1746	0	-	1.94	4.29
LER	vertical	8	3.109	3.159	1746	0	1.18	2.34	5.32
LER	vertical	6	3.109	3.159	1746	2	-	2.00	3.22
LER	vertical	8	3.109	3.159	1746	2	1.13	2.45	4.10
LER	vertical	6	2.5	3.159	1746	-3	-	1.58	5.92
LER	vertical	8	2.5	3.159	1746	-3	-	1.81	6.88
LER	vertical	6	2.5	3.159	1746	0	1.39	2.95	6.32
LER	vertical	8	2.5	3.159	1746	0	1.66	3.61	7.47
LER	vertical	6	2.5	3.159	1746	2	1.20	2.64	4.32
LER	vertical	8	2.5	3.159	1746	2	1.45	3.32	5.49

Table 9: De-Qing necessary to fix instability due to cavity higher-order modes, when the BPM resonance is removed.

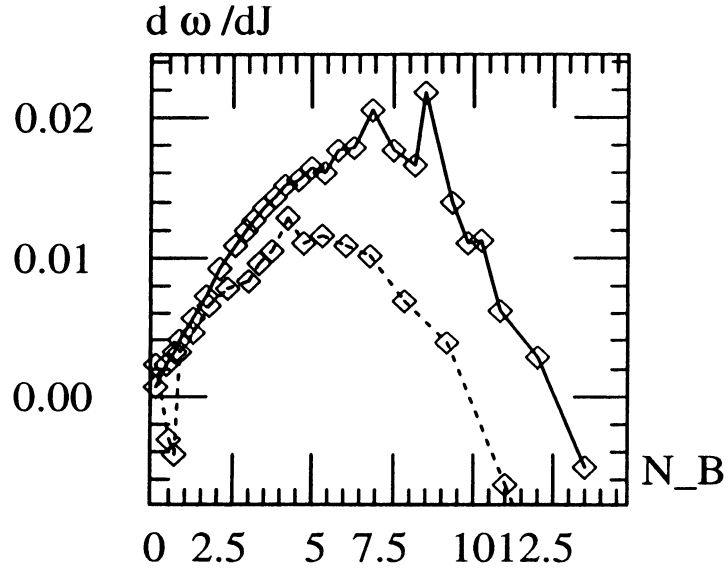


Figure 4: Tune shift with amplitude computed for a single bunch, plotted versus number of particles in a bunch. This is done for the low energy ring at 3.109 GeV [Hei].

Also, it should be noted that the way Landau damping was computed (using the method of [ZCB86]) may need to be re-examined or re-computed in the context of the method of [Ber96a]. Its interaction with mode coupling and chromaticity is not clear.

I should emphasize that one cannot ignore mode coupling in this calculation. Mode coupling gives a significant effect, probably making the cavities significantly more difficult to damp.

References

- [ASM90] ASM International Handbook Committee, Materials Park, Ohio. *Metals Handbook*, tenth edition, 1990.
- [Ber95a] J. Scott Berg. Observations involving broadband impedance modelling. Technical Report SLAC-PUB-95-6964, Stanford Linear Accelerator Center, Stanford, California, August 1995. To appear in the proceedings of the International Workshop on Collective Effects and Impedance for B-Factories, Tsukuba, Japan, 12–17 June, 1995.
- [Ber95b] J. Scott Berg. Transverse multibunch head-tail mode growth rates in the pep-ii b-factory. Technical Report PEP-II AP Note 95.16, SLAC, Stanford, CA, July 1995.
- [Ber96a] J. Scott Berg. *Coherent Modes for Multiple Non-Rigid Bunches in a Storage Ring*. PhD thesis, Stanford University, Stanford, CA, March 1996. SLAC report SLAC-R-478.
- [Ber96b] J. Scott Berg. Documentation for v1asov version 0.1. Technical Report SLAC-TN-96-1, SLAC, Stanford, CA, March 1996.
- [BR95a] J. Scott Berg and Ronald D. Ruth. Transverse instabilities for multiple nonrigid bunches in a storage ring. *Phys. Rev. E*, 52(3):R2179–2182, September 1995.
- [BR95b] J. Scott Berg and Ronald D. Ruth. Transverse multibunch modes for non-rigid bunches, including mode coupling. Technical Report SLAC-PUB-95-6965, SLAC, Stanford, CA, August 1995.
- [Cai] Yunhai Cai. Private communication.
- [Cha93] Alexander Wu Chao. *Physics of Collective Beam Instabilities in High Energy Accelerators*. John Wiley & Sons, Inc., New York, 1993.
- [Chi94] Y. H. Chin. User’s guide for ABCI version 8.8 (azimuthal beam cavity interaction). Technical Report LBL-35258, Lawrence Berkeley Laboratory, Berkeley, CA, February 1994.
- [Dal] Ed Daley. Private communication.
- [GvZZ93] Robert L. Gluckstern, Johannes van Zeijts, and Bruno Zotter. Coupling impedance of beam pipes of general cross section. *Phys. Rev. E*, 47(1):656–663, January 1993.
- [Hei] Sam Heifets. Private communication.
- [HK89] S. A. Heifets and S. A. Kheifets. High-frequency limit of the longitudinal impedance of an array of cavities. *Phys. Rev. D*, 39(3):960–970, February 1989.
- [HKL⁺95] S. Heifets, K. Ko, X. Lin, A. Chao, G. Stupakov, M. Zolotarev, J. Seeman, U. Weinands, C. Perkins, M. Nordby, E. Daly, N. Kurita, D. Wright, E. Henestroza, G. Lambertson, J. Corlett, J. Byrd, M. Zisman, T. Weiland, W. Stoeffl, and C. Belsler. Impedance study for the PEP-II B-factory. Technical Report SLAC/AP-99, Stanford Linear Accelerator Center, Stanford, CA, March 1995.
- [Hun] Don Hunt. Private communication.
- [Ng] Cho Ng. Private communication.
- [PEPa] PEP-II machine advisory committee meeting, August 24–25, 1995.

- [PEPb] PEP-II machine advisory committee meeting, January 4–6, 1995.
- [PEP93] PEP-II an asymmetric B factory, conceptual design report. Technical Report SLAC-418, LBL-PUB-5379, CALT-68-1869, UCRL-ID-114055, UC-IIRPA-93-01, 1993.
- [Rim] Robert Rimmer. Private communication.
- [Sch] Heinz Schwarz. Private communication.
- [ZCB86] M. S. Zisman, S. Chattopadhyay, and J. J. Bisognano. ZAP user's manual. Technical Report LBL-21270 and UC-28, Lawrence Berkeley Laboratory, Berkeley, CA, December 1986.